

High-pressure study of the ground- and superconducting-state properties of CeAu_2Si_2

Gernot W. Scheerer* and Gaétan Giriat

DQMP - University of Geneva, 24 Quai Ernest-Ansermet, 1211 Geneva 4, Switzerland.

Zhi Ren

Institute for Natural Sciences, Westlake Institute for Advanced Study, Hangzhou, P. R. China.

Gérard Lapertot

SPSMS, UMR-E 9001, CEA-INAC/UJF-Grenoble 1, 38054 Grenoble, France.

Didier Jaccard

DPMQ - University of Geneva, 24 Quai Ernest-Ansermet, 1211 Geneva 4, Switzerland.

(Dated: April 5, 2024)

The pressure-temperature phase diagram of the new heavy-fermion superconductor CeAu_2Si_2 is markedly different from those studied previously. Indeed, superconductivity emerges not on the verge but deep inside the magnetic phase, and mysteriously T_c increases with the strengthening of magnetism. In this context, we have carried out ac calorimetry, resistivity, and thermoelectric power measurements on a CeAu_2Si_2 single crystal under high pressure. We uncover a strong link between the enhancement of superconductivity and quantum-critical-like features in the normal-state resistivity. Non-Fermi-liquid behavior is observed around the maximum of superconductivity and enhanced scattering rates are observed close to both the emergence and the maximum of superconductivity. Furthermore we observe signatures of pressure- and temperature-driven modifications of the magnetic structure inside the antiferromagnetic phase. A comparison of the features of CeAu_2Si_2 and its parent compounds CeCu_2Si_2 and CeCu_2Ge_2 plotted as function of the unit-cell volume leads us to propose that critical fluctuations of a valence crossover play a crucial role in the superconducting pairing mechanism. Our study illustrates the complex interplay between magnetism, valence fluctuations, and superconductivity.

I. INTRODUCTION

Although known about for many years, heavy fermion (HF) systems are still intensely studied since they unite some of the most interesting features of strongly correlated electron systems such as quantum criticality, non-Fermi-liquid behavior, and unconventional superconductivity. In this context, the antiferromagnet CeAu_2Si_2 presents new challenges to the current understanding of HF superconductivity. In CeAu_2Si_2 [1], the magnetic and superconducting phases overlap across an unprecedentedly broad pressure range from $p = 11.8$ GPa up to the critical pressure $p_c \sim 22.5$ GPa, where the superconducting transition temperature T_c is highest, as shown in the schematic phase diagram in Fig. 1(a). Contrary to all previous observations, both T_c and the magnetic ordering temperature increase simultaneously over an extended pressure range. Thus, at low temperatures, CeAu_2Si_2 behaves very differently from the isostructural and iso-electronic parent compounds CeCu_2Si_2 and CeCu_2Ge_2 . In contrast, all three systems exhibit remarkably similar properties at intermediate and high temperatures.

Among the Ce-based HF superconductors, CeAu_2Si_2 displays one of the highest T_c of ≈ 2.5 K. Superconductivity (SC) appears to involve HF quasiparticles with an effective mass $m^* \approx 100 m_e$, as inferred from the large

initial slope of the upper critical field [1]. Furthermore, the strong pair-breaking effect of non-magnetic impurities attests unconventional SC [2]. CeAu_2Si_2 has a tetragonal ThCr_2Si_2 -type structure with the space group $I4/mmm$ (D_{4h}^{17}) [3, 4] and orders antiferromagnetically below $T_N = 9.6$ K [5, 6]. The resistivity [Fig. 1(b)] and thermopower exhibit typical Kondo lattice behavior [7–9]. The ambient-pressure ground state is an A-type antiferromagnetic (AF) structure with a magnetic moment oriented along the \mathbf{c} -axis of $(1.29 \pm 0.05) \mu_B$ at 5 K [4]. The Sommerfeld coefficient $\gamma = 11$ mJ/K²·mol and the AF energy gap $\Delta = 7.5$ K are determined by fitting the low-temperature ($T < 5$ K) specific heat [6]. The valence of the Ce ion is 3.00 [4] and the estimated Kondo temperature is $T_K = 1.7$ K [10]. T_K increases by roughly 1-2 orders of magnitude when a hydrostatic pressure of 15 GPa is applied [11]. Inelastic magnetic peaks in the neutron scattering spectra show crystal field excitations [12, 13]. A magnetic field of 5.5 T applied along the magnetic easy axis \mathbf{c} is sufficient to suppress the AF order and leads to a polarized paramagnetic state via a metamagnetic transition [6, 14, 15]. Furthermore, as observed in specific heat and magnetization experiments [6], CeAu_2Si_2 exhibits two successive magnetic transitions at 8.0 and 9.6 K, which separate the AF ground state from the paramagnetic state.

Concerning the effect of pressure, it is noteworthy that the AF transition line T_N is nonmonotonic forming a triple dome [see Fig. 1(a)], which suggests pressure-

* gernot.scheerer@unige.ch

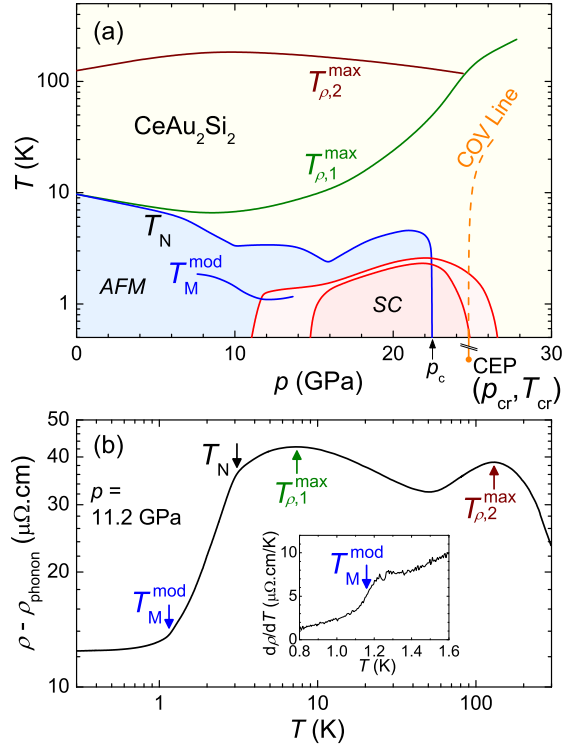


FIG. 1. (a) Schematic pressure-temperature phase diagram of CeAu_2Si_2 based on Refs. [1] and [2] and this work. (b) Resistivity ρ versus temperature T of CeAu_2Si_2 at 11.2 GPa. The phonon term was subtracted. Inset: $d\rho(T)/dT$ around the anomaly at T_M^{mod} .

induced modification of the magnetic structure. Moreover, the crossover line corresponding to the delocalization of 4f electrons (labeled COV below) is located just above p_c [see Fig. 1(a)] [1, 2]. The rapid collapse of magnetism and the SC enhancement may be driven by critical valence [16] or even orbital [1] fluctuations.

To refine the high-pressure phase diagram of CeAu_2Si_2 , we performed measurements up to 24.3 GPa on a single crystal using techniques presented in Refs. [17, 18] providing nearly hydrostatic pressure conditions. Using a multiprobe setup, we examined the in-plane electric resistivity, in-plane thermoelectric power, and ac calorimetry. With magnetic fields applied along the c-axis, we examined the pressure dependence of the superconducting upper critical field H_{c2} and its initial slope $dH_{c2}/dT|_{T \rightarrow T_c}$, as well as the pressure dependence of the normal-ground-state properties for $H > H_{c2}$. The present work confirms the existing phase diagram [1] and reveals the following major novelties. i) A new transition line T_M^{mod} , presumably due to the reconstruction of magnetic order, is observed inside the AF phase [see Fig. 1(a)]. Corresponding anomalies are clearly seen, e.g. in the resistivity [Fig. 1(b) and inset]. ii) Intriguingly, while T_N decreases with increasing pressure, the magnetic phase becomes much more stable in a magnetic field. iii) Comparing the magnetic-transition lines with the large superconducting

dome reveals that both the emergence of SC deep inside the AF phase and the maximum T_c occur close to magnetic instabilities in two “critical” pressure regions. The first region around 14 GPa corresponds to a minimum in T_N and enhanced electronic scattering rates. The second one around 22 GPa is marked by the abrupt vanishing of magnetism, quantum-critical-like signatures, and non-Fermi-liquid (NFL) behavior. This corroborates the idea that the SC in CeAu_2Si_2 is driven by quantum critical fluctuations.

This paper is organized as follows. Section II presents the experimental methods. In Sect. III, we present the results of our multiprobe experiment. Section III A focuses on the identification of the phase transitions in the pressure region of emerging SC, Sect. III B shows details of the thermopower, and Sect. III C presents the pressure-temperature phase diagram and the normal-ground-state properties. In Sect. IV, we discuss the experimental results and the possible superconducting pairing mechanism.

II. EXPERIMENT

We performed measurements on a Sn-flux-grown CeAu_2Si_2 single crystal in a standard dilution fridge equipped with a superconducting magnet coil with a maximum field of 8.5 T. Details of the crystal growth are described in Ref. [1]. To generate pressure, we used a Bridgman-type sintered-diamond-anvil pressure cell with a pyrophyllite gasket and steatite as a soft-solid pressure medium. Pressure was determined from the resistive T_c of a lead strip. The pressure gradient along the sample, estimated from the Pb-transition width, slowly increased from ≈ 0.5 GPa at low pressure to ≈ 0.8 GPa at maximum pressure. The four-point resistivity was measured with a dc current along the sample basal plane. For dc thermoelectric power and ac calorimetry measurements, a local heater very close to one sample extremity provided a temperature gradient and temperature oscillations, respectively. The thermoelectric voltages were measured by pairs of Au and $\text{AuFe}_{0.07\%}$ wires. Technical details can be found in Refs. [1, 17] and [18]. The superconducting transition temperatures are defined as i) T_c^{onset} at twice the noise deviation from a straight tangent to the normal-state resistivity just above T_c and ii) T_c^{bulk} at the midway anomaly in calorimetry. Quantities labeled as normal-state properties were obtained by applying a magnetic field corresponding to the upper critical field of the resistive-SC-transition onset ($\approx 1.4 \cdot H_{c2}$, see Fig. 9 later). It was verified experimentally that the normal-state properties are qualitatively independent of the magnetic field up to 8.5 T.

III. RESULTS

A. Magnetic transitions

Figure 2 displays low-temperature data measured with the multiprobe setup in the vicinity (i.e., below and above the pressure) of the SC emergence. Generally, the anomaly at the Néel temperature T_N is clearly visible in the ac calorimetry and resistivity. At 13.6 GPa, resistivity [Fig. 2(a)] shows an incomplete superconducting transition with $T_c^{\text{onset}} \approx 1.4$ K, while at 16.5 GPa, the transition is complete and also seen in the thermopower [Fig. 2(d)]. Moreover, calorimetry [Fig. 2(c)] has the signature of bulk SC at $T_c^{\text{bulk}} = 1.6$ K. T_c^{bulk} (T_c^{onset}) reaches its maximum of 2.2 K (2.6 K) at 20.4 GPa.

In addition to the superconducting and AF transitions, the probes reveal other anomalies. At a temperature T_M^{mod} , the calorimetry exhibits a bump [see Fig. 2(c) and upper inset] and the resistivity exhibits a kink, corresponding to an abrupt jump in the temperature derivative $d\rho/dT$ [see Fig. 2(b)]. These anomalies are observed in the pressure range 7.6 – 13.6 GPa, i.e., well inside the AF phase. Their sharpness is characteristic of a phase transition and it is clear that they are not due to SC since they persist in magnetic fields higher than $H_{c,2}$. As discussed below, the anomalies in C^{ac} and $d\rho/dT$ correspond to the same phenomenon, most likely to a magnetic transition (therefore the label T_M^{mod}). Moreover, the thermopower [Fig. 2(d)] shows a local maximum at T_S^{max} close to T_M^{mod} , which persists over the whole pressure range.

Figures 3(a) and 3(b) show for $p = 11.2$ GPa, a decrease in T_M^{mod} with increasing magnetic field $\mathbf{H} \parallel \mathbf{c}$, revealed via ρ and $d\rho/dT$. T_M^{mod} becomes more field-resistant with increasing pressure: while T_M^{mod} is suppressed by roughly 9 T at $p = 11.2$ GPa, the anomaly seems to persist well above 10 T at 13.6 GPa [see Fig. 3(c)]. Similarly, the H dependence of the Néel temperature T_N [e.g., for $p = 13$ GPa in Fig. 3(c)] reveals an unusual behavior of magnetism in CeAu₂Si₂. Despite T_N rapidly decreasing with increasing pressure, the magnetic phase becomes much more stable against the magnetic field. At zero pressure, $T_N = 10$ K and the metamagnetic transition field is $H_c = 5$ T, but at pressures above 7 GPa, where $T_N \approx 3$ K, the AF phase survives far beyond 8 T. A similar p -induced increase in H_c has been observed for CeRh₂Si₂ [19] and seems to be related to a p -induced modification of the magnetic structure [20]. Figure 3(d) shows that the field dependences of T_M^{mod} deduced from resistivity and calorimetry are identical, indicating that the corresponding anomalies are caused by the same phenomenon: the transition at T_M^{mod} . Additionally, the temperature T_S^{max} of the maximum thermopower shows exactly the same behavior. The field dependence of T_M^{mod} is similar to that of T_N but clearly different than that of the superconducting T_c^{onset} . Following a recent study of CeIn₃ [21], we assume the relationship $T_N(H) = T_{N,0}[1 - (H/H_c)^2]$, where $T_{N,0}$ is the

zero-field transition temperature and H_c is the critical field. At $p = 13$ GPa, the extrapolated H_c value for T_N is roughly 30 T and an analogous relationship for T_M^{mod} yields 14 T. The similarity of the field dependences of T_N and T_M^{mod} indicates that the anomalies at T_M^{mod} are induced by reconstruction of the AF order, as observed at zero pressure at $T_{N,3} = 8.0$ K [6].

B. Thermoelectric power

Figure 4 presents the normal-state ($H > H_{c2}$) thermopower S and S/T as a function of temperature (below 6 K) for different pressures. Between 7.6 and 13.6 GPa, S is negative and exhibit a local maximum or a shoulder at T_S^{max} . Additionally, a local minimum occurs at $T_S^{\text{min}} < T_S^{\text{max}}$ for intermediate pressures [see Fig. 5(a) for the p dependence of T_S^{max} and T_S^{min}]. Since the local maximum becomes positive for $p \geq 14.7$ GPa, S crosses the zero line twice up to 16.5 GPa. Above T_S^{max} , S decreases continuously with increasing T and the temperature, at which its sign changes to negative, increases with pressure. Furthermore, T_S^{max} and the magnitude of S at T_S^{max} increase strongly with pressure when $p \gtrsim 20$ GPa. The pressure dependence of the S isotherm at 4 K [Fig. 5(b)] is in good agreement with our previous study [11]. Similar to S , S/T exhibits a maximum at the temperature $T_{S/T}^{\text{max}}$, which culminates at 18.3 GPa, and vanishes abruptly at higher pressure [see Fig. 5(a)]. Actually, $T_S^{\text{max}} \approx T_{S/T}^{\text{max}}$ at low pressures, but these two temperatures diverge for high pressures. Note that the behavior of S is qualitatively different for pressures above 20 GPa, where S/T decreases continuously with T . For $T \rightarrow 0$, S tends to recover a linear T dependence and its initial slope $S/T|_{T \rightarrow 0}$ can be approximated, although systematic measurements down to still lower temperature are desirable for a better determination. Nevertheless, Fig. 5(b) reveals that $S/T|_{T \rightarrow 0}$ exhibits a narrow maximum of $\approx 10 \mu\text{V/K}^2$ located slightly above p_c . $S/T|_{T \rightarrow 0}$ continues to decrease beyond 25 GPa, as shown by data from Ref. [11], reflecting the increasing hybridization of Ce-4f and conduction electrons.

Inside the AF phase, negative and positive contributions to S result in subsequent local minimum and maximum, respectively, which is most clearly demonstrated for $p = 14.7$ GPa. A local extrema can be attributed to an AF gap: a minimum (maximum) is due to a gap below (above) the Fermi level and $e > 0$ ($e < 0$) [22]. In the present case, a putative reconstruction of the AF order with a change in the gap structure at $T_M^{\text{mod}} \lesssim T_S^{\text{max}}$ most likely induces the oscillation of S below T_N . The plot of S versus T/T_N [Fig. 6(a)] shows that the oscillating behavior is already observed at zero pressure (data from another sample), where more marked anomalies can be brought into connection with the transitions at $T_{N3} = 8.0$ K and $T_N = 9.6$ K observed in the specific heat [6]. Thus, the features in the thermopower corroborate the interpretation of the T_M^{mod} anomalies in the resistiv-

ity and calorimetry. Furthermore, $T_{S/T}^{\max}$ shows field and pressure dependences [Figs. 3(d) and 5(a)] very similar to those of T_N and T_M^{mod} , underlining their coupling.

Let us now comment on the observation that $T_{S/T}^{\max}$ drops to zero just above 18.3 GPa, while T_S^{\max} persists and rises strongly at higher pressures [see Fig. 5(a) and also Ref. [11]]. A feature in $S(T)$, induced by a phenomenon such as a magnetic rearrangement, is expected to persist in $S(T)/T$. This is clearly the case of the low-pressure maximum (and minimum), whereas the high-pressure maximum occurs only in S but not in S/T . Therefore, the maximum in S at the highest pressures is not related to a magnetic transition but rather to a crossover. Further evidence for that the low- and high-pressure maxima have different origins is the field dependence of their magnitude [see Fig. 6(b)]. For $p \leq 18.3$ GPa, the magnitude of S exhibits no or slightly negative field dependence. By contrast, for higher pressures, the magnitude shows a sizable increase at $\mu_0 H = 8$ T. The high-pressure maximum presumably marks a crossover between a positive zero- T term and a negative intermediate- T contribution. We conclude that the low- and high-pressure maxima in S have to be distinguished.

C. Phase diagram and normal-state properties

Figure 7(a) presents the pressure-temperature phase diagram of CeAu_2Si_2 obtained from the calorimetry, resistivity, and thermopower results. First, let us clarify two points: i) although there is no proof from microscopic probes, we consider that the high-pressure phase below T_N is AF, which means that there is an unexpected resurgence of the AF-transition line under pressure. This is supported by the continuity of the characteristic anomalies in the calorimetry and resistivity at T_N . ii) T_N and T_M^{mod} data points below T_c^{onset} are obtained from the normal state ($H > H_{c2}$) and there is not yet any evidence for the coexistence of SC and AF order. Concerning T_N and the superconducting dome, the new phase diagram is in perfect agreement with the previous one [1], except for a minor downward pressure shift of ≈ 1 GPa.

The Néel temperature T_N rapidly decreases from 9.6 K at zero pressure down to 3 K at 7.6 GPa. Here, an abrupt upturn results in a first maximum at 10 GPa. It follows a minimum ($T_N = 2.5$ K) and a second upturn at 14.7 GPa, above which T_N strongly increases to a maximum of 4.5 K at 19.5 GPa. Finally, the magnetic order vanishes at $p_c \sim 22$ GPa. Given that the pressure gradient along the sample is ≈ 0.8 GPa at p_c , the sudden collapse of T_N is first-order like. The transition line T_M^{mod} is established from 7.6 to 13.6 GPa. Starting at $T_M^{\text{mod}} = 1.85$ K, it decreases to ~ 1.1 K. The behavior of T_M^{mod} clearly mimics that of T_N (at about 1 K lower), indicating a magnetic origin.

The strongly modified field dependence and the peculiar pressure dependence of T_N suggest that the low-,

intermediate-, and high-pressure magnetic ground states of CeAu_2Si_2 are different, with subsequent modifications of the propagation wave vector and Brillouin zone at ~ 8 and ~ 15 GPa, respectively. Magnetic order may change from long-range localized- to itinerant-moment magnetism. As observed at a similar unit-cell volume in CeCu_2Si_2 , CeCu_2Ge_2 , and $\text{CeCu}_2(\text{Si}_{1-x}\text{Ge}_x)_2$ alloys, the high-pressure ordering wave vector may be incommensurate [23–25]. In fact, the reconstruction of magnetically ordered phases induced by different control parameters is commonly observed in Ce-HF compounds. Examples are the effect of external pressure on CePb_3 [26] and CeRh_2Si_2 [20, 27] or the alloying (chemical pressure) in CeCu_2Si_2 leading to the observation of three AF phases with different propagation vectors [25, 28].

Partial SC emerges around 12.7 GPa and T_c^{onset} increases linearly almost up to the maximum of the superconducting dome. It is most noteworthy that T_c^{onset} increases simultaneously with T_N over a considerable pressure range of ≈ 6 GPa. Bulk SC emerges at 15.5 GPa and T_c^{bulk} rises in parallel with T_c^{onset} up to a maximum of 2.2 K. The maximum T_c at 20.4 GPa is close to the collapse of magnetism at p_c . The bulk SC spans over 9 GPa and the partial SC spans a huge p -domain of over 17 GPa including data from Ref. [1]. The resistive transition is very large at the emergence and evanescence of SC. In the region of bulk SC, the transition width is at least 0.4 K, i.e., 0.1 K more than that in Ref. [1], where good agreement was found between T_c^{bulk} and zero-resistivity. By contrast, the parent compounds CeCu_2Si_2 [29, 30] and CeCu_2Ge_2 [31] exhibit narrow transitions at pressures close to the emergence (p_c) or maximum (p_v) of SC, while the transition is broad not only at the decrease in SC but also at intermediate pressures. The large regions of partial SC are presumably due to exotic superconductivity, such as textured SC, as observed in CeRhIn_5 [32] or limited to the surface as we proposed [33] for CeCu_2Si_2 .

Figures 7(b) – 7(d) display salient features of the resistivity, which correlate with the two “critical” regions of the phase diagram, i.e., the regions of the minimum T_N and the collapse of magnetism, respectively. As usual, the normal-state resistivity [$H > H_{c2}$, Fig. 8(a)] is analyzed using the equation of a gapped spin-wave antiferromagnet [34] for $p < p_c$ [see Fig. 8(b)] and the power law $\rho = \rho_0 + A \cdot T^n$ for $p > p_c$. The residual resistivity ρ_0 exhibits a shoulder at 13 GPa and a maximum at 20 GPa, while the A coefficient has two maxima at higher pressures by about 2 GPa [see Fig. 7(b)]. Below p_c , due to magnetic coherent electron scattering, A is reduced roughly by a factor of 8 compared with a hypothetical nonmagnetic-ground-state value, which is indeed that observed in CeCu_2Si_2 [29] and CeCu_2Ge_2 [31] at their p_c . It is noteworthy that the pressure dependence of the AF energy gap Δ closely follows that of T_N [Fig. 7(d)]. Enhanced electronic scattering rates around 14 GPa may be related to a magnetic instability indicated by the minimum T_N and T_M^{mod} . The anomaly in ρ_0 is relatively weak, although the shoulder in ρ_0 has a similar amplitude to

that at p_c in the parent compound CeCu_2Ge_2 [31]. Moreover, the pressure dependence of the isothermal resistivity at temperatures above T_N [Fig. 7(c)], which is used to probe the ground-state excitations independently of magnetic ordering, confirms enhanced scattering around 14 GPa. Indeed, at $T = 5$ K, the ρ -isotherm exhibits a broad peak at 16.5 GPa, which is shifted to 15.5 GPa by lowering the temperature to 3.5 K. By continuity, this peak becomes the shoulder in ρ_0 at 13 GPa. In addition, the extrapolation of the low-pressure T_N line [1, 9] collapses at ~ 15 GPa. All these features including the maximum A may reflect enhanced magnetic instabilities, which do not lead to a true quantum critical point (QCP) because of the sudden strengthening of magnetism above 14.7 GPa. Thus, only a few characteristics of spin-mediated SC are found in this p -region.

In the second region, i.e., around p_c , the large enhancement in ρ_0 indicates quantum critical fluctuations [35]. The maximum ρ_0 at 20 GPa occurs slightly below the magnetic collapse at $p_c = 22$ GPa. The sharp anomaly in A at p_c can be explained as follows. A rises abruptly just below p_c since paramagnetic Ce 4f-electron scattering is recovered after the collapse of the magnetic order. The considerable reduction in A between 21.5 and 24.3 GPa is caused by both the collapse of spin fluctuations and the increasing itinerant character of Ce 4f electrons, as in the cases of CeCu_2Si_2 and CeCu_2Ge_2 at p_v [31]. Including the data from Ref. [1], A decreases by two orders of magnitude up to 27.6 GPa. Furthermore, around p_c , the exponent n [Fig. 8(c)] exhibits clear NFL behavior. At $p = 21.5$, 23.1, and 24.3 GPa, n is close to 1.5 and constant up to roughly 10 K. Defining T_{PL} as the temperature below which the power law $\rho - \rho_0 = T^n$ with $1 < n < 2$ holds, it is striking that $T_{PL} \approx 17$ K is maximum at $p = 23.1$ GPa, i.e., slightly above p_c [see Fig. 8(d)]. Lastly, Fermi liquid behavior ($n = 2$) is recovered below the usual temperature scale T_{FL} for $p \geq 24.3$ GPa.

Figure 9 presents properties of the upper critical field H_{c2} (defined by a 95% drop in resistivity). H_{c2} and its initial slope $H'_{c2} = -dH_{c2}/dT|_{T \rightarrow T_c}$ show p dependences similar to that of T_c^{bulk} , i.e., a dome shape around $p = 20.4$ GPa with maximum values of 6.8 T and 11.8 T/K, respectively. From the emergence of bulk SC to the maximum T_c , H'_{c2} is enhanced by roughly a factor of 2, indicating in the clean limit an enhancement of the effective mass m^* by 40%.

To summarize, clear signatures of quantum critical behavior around p_c are found in the normal-state ρ and in all probes sensitive to m^* . The quantities A , $S/T|_{T \rightarrow 0}$, and H'_{c2} show similar variations, i.e., a strong peak close to p_c and a rapid decrease at higher pressures. However, the peak positions of these quantities are spread over pressures from 20.4 to 23.1 GPa. This difference in p is rather large in comparison with the usual p scale of HFs and cannot be explained alone by the pressure gradient $\Delta p < 1$ GPa along the sample. The dispersion of the peak positions over the pressure axis is signifi-

cant and one can not simply attribute all the features in the normal- and superconducting-state properties to one isolated QCP. Indeed, below we discuss the interplay between the collapse of magnetism at p_c and the critical endpoint of the COV line at a slightly higher p_{cr} .

IV. DISCUSSION

Figure 10 presents a schematic plot of the characteristic temperatures of CeCu_2Si_2 , CeCu_2Ge_2 , and CeAu_2Si_2 versus the unit-cell volume V , which highlights the striking similarities between these systems. Such a comparison was previously elaborated in Ref. [1]. In particular, CeCu_2Ge_2 under a pressure of ≈ 10 GPa coincides perfectly with CeCu_2Si_2 at ambient pressure and only data of the latter are shown for $V < 163 \text{ \AA}^3$. The three compounds show a broad overlap of their superconducting regions. The energy scales $T_{\rho,1}^{\text{max}}$ due to Kondo scattering and $T_{\rho,2}^{\text{max}}$ due to scattering on the excited crystal field levels (see also Fig. 1) merge at $V = 159 \text{ \AA}^3$ and the maximum T_c occurs near this volume. Thus, T_c is highest when the Kondo and CEF-splitting energies become comparable. The Kondo temperature T_K , identified as the main parameter, drives the systems from long-range magnetic ordered states, through SC, towards a strongly delocalized paramagnetic f -metal at a reduced volume. At pressures where the SC is strongest, the system is controlled by a relatively high energy scale: $T_K \approx T_{\rho,2}^{\text{max}}$. Clearly, similarities in Fig. 10 underline the key role of the local Ce ion environment. However, for a given volume V the crystallographic parameters a and c slightly vary by $\approx 1\%$ between the systems [36–38], although Cu and Au are isovalent. Obviously Au possesses a different atomic potential from copper. Substituting Au for Cu triples the atomic mass and increases the valence shell quantum number from 3 to 5, adding extra 5d electrons.

Only a few significant differences are found between CeAu_2Si_2 and $\text{CeCu}_2\text{Si}_2/\text{CeCu}_2\text{Ge}_2$. The most important are the twofold enhancement of $T_{\rho,2}^{\text{max}}$, the large overlap of SC with AF order, the magnetism spanning to a lower unit-cell volume V , and the SC extending to a higher V . These differences require explanation and may be pertinent for understanding the nature of the superconducting pairing mechanism. Actually, the twofold enhancement of $T_{\rho,2}^{\text{max}}$ may be the crucial point, indicating that the substitution of Cu by Au significantly changes the crystal-field environment of the Ce-4f-moments, affecting the ground-state properties of the system.

In agreement with the standard behavior of Ce-based HF superconductors, the maximum T_c of CeAu_2Si_2 is close to the pressure p_c where the magnetic order vanishes. By contrast, CeCu_2Si_2 and CeCu_2Ge_2 appear to be exceptions since their T_c peaks are far above their p_c . However, for CeCu_2Ge_2 there is one report [39] of an ordering temperature persisting to a higher pressure, indicating a p_c closer to T_c^{max} .

We now add new aspects to the comparison of

CeCu₂(Si/Ge)₂ and CeAu₂Si₂.

i) The thermopower of all three systems exhibits a low- T peak or shoulder. We have argued above that for CeAu₂Si₂ these features have different origins below and above p_c . For $p < p_c$, the maximum of S in CeAu₂Si₂ and CeCu₂Ge₂ [17, 40] occurring below T_N is related to the opening of an AF spin gap, and its temperature scale collapses just before p_c . For $p > p_c$, the low- T maximum of S occurs deep inside the coherent regime and seems to be unrelated to the Kondo effect, although its temperature scale T_S^{\max} increases strongly with p . Indeed, T_S^{\max} in Fig. 10 (data of CeCu₂Si₂ in Refs. [42] and [43]) is much lower than $T_{\rho,1}^{\max} \propto T_K$, and is even below the Fermi liquid temperature T_{FL} in CeAu₂Si₂. Moreover, we note the very low T_S^{\max} value in CeCu₂Si₂ just above p_c . Concerning the origin of T_S^{\max} for $p > p_c$ we consider two possibilities. On one hand, T_S^{\max} might be due to the development of magnetic correlations with decreasing T , or on the other hand it can signal the crossover between the zero- T -limit term $S \propto \gamma T$ [44] and the usual Kondo term as described by theory [45].

ii) Recently, Seyfarth *et al.* [29] established, by resistivity scaling, the COV line in the p - T plane of CeCu₂Si₂ with a critical end point at p_{cr} and at a slightly negative temperature T_{cr} [see also Fig. 1(a)]. This crossover is ascribed to a pressure-induced change in the Ce 4f ion valence. Similar scaling behavior and the resulting COV line have also been reported for CeAu₂Si₂ with $p_{cr} = 23.6$ GPa and $T_{cr} = -14$ K [1]. It is of upmost importance that the COV lines shown in Fig. 10 occur at almost the same V for the three systems (the shift of -1 Å³ is within the experimental error). This V is slightly lower than that where $T_{\rho,1}^{\max}$ and $T_{\rho,2}^{\max}$ coincide.

iii) For all three systems, the most pronounced NFL behavior of $\rho(T)$ is observed in the vicinity of the COV, i.e., slightly above p_c for CeAu₂Si₂. At p_{cr} , the free-exponent-power-law scale T_{PL} has a peak value of 6 to 10 times the superconducting T_c^{\max} as sketched in Fig. 10. For CeCu₂(Si/Ge)₂, the minimum power-law exponent is $n = 1$ at the pressure of T_c^{\max} [18, 31], while n is never lower than ≈ 1.5 in CeAu₂Si₂.

iv) The red dashed-dotted line in Fig. 10 represents the superconducting T_c^{onset} of a self-flux-grown CeAu₂Si₂ crystal with a similar T_N line, identical p_c , but a much larger residual resistivity ρ_0 (compared to a low- ρ_0 , Sn-flux-grown sample) [2]. The SC dome of this sample has only half the width of that of a low- ρ_0 sample and SC is absent for $V > 163$ Å³, which corresponds to the observed p_c in CeCu₂(Si/Ge)₂. Moreover, the maximum T_c^{bulk} of the three systems displays the same reduction versus ρ_0 , indicating pair breaking by nonmagnetic disorder [2]. Such an effect appears to be even stronger for $V > 163$ Å³, which suggests that SC is not yet observed in CeCu₂Ge₂ for $p < 10$ GPa or in partially Ge-substituted CeCu₂Si₂ [25, 46] because of the too short mean free path $l \propto \rho_0^{-1}$ in the investigated samples.

We now discuss the origin of SC in CeAu₂Si₂. Since the first high-pressure investigation of CeCu₂Si₂, the T_c

dome was first associated with the instability of the Ce ion valence [47] and subsequently ascribed to charge fluctuations [31] following Miyake and coworkers, who clarified conditions for a pairing mechanism based on critical valence fluctuations [18, 48–51]. Later on, Yuan *et al.* [46] found by Ge alloying at the Si site of CeCu₂Si₂ that the SC dome is a combination of two distinct states centered at p_c and p_v . The underlying pairing mechanism of the high- T_c region around $p_v \gg p_c$ was thought (and this is still the dominant view) to be different from that of the low- T_c pocket around p_c [16, 18, 29, 52–55]. Because of the multiple similarities (some are shown in Fig. 10, but there are others, such as the value of the FL coefficient $A \propto 1/T_{\rho,1}^{\max}$ [1] and the thermopower behavior for $T < 300$ K [11]), an analogous situation is expected for CeCu₂Ge₂ and CeAu₂Si₂. By taking this approach, we first examine the emergence of SC.

One key point is that in CeAu₂Si₂, partial and bulk SC emerge at pressures close to the minimum T_N . Despite the extrapolation of T_N from $p < 7$ GPa suggesting a QCP around 15 GPa, the observed magnetic line does not collapse here but at a much higher pressure. Thus, our results diverge from the general consensus that the SC in a HF emerges near the verge of magnetism [56]. The enhanced scattering rates around the minimum T_N [see Figs. 7(b) and 7(c)] support the idea that Cooper pairs are formed by magnetic fluctuations, which has been proposed to be the case for the low- T_c state in CeCu₂Si₂ [57, 58]. However, let us recall that for this system the scenario of a spin-mediated SC, more precisely, of a nodal d-wave order parameter, has been increasingly challenged, notably by the results of thermodynamic measurements [59] and theoretical calculations [60].

Then, when SC has set in, T_c considerably increases with the strengthening of magnetism over a large V interval, contrary to all previous observations. In this broad p -region, it seems that SC does not compete with magnetism, as always considered but, rather, both phenomena occur in a complementary manner over an interval comparable to or larger than the total superconducting region of other HFs. On the other hand, the partial collapse of T_M^{mod} slightly precedes the emergence of SC. Our experiment does not reveal, whether there is spatial segregation between superconducting and magnetically ordered domains or whether the SC expels magnetism. Both cases would require that SC and magnetism do not interact on a microscopic scale. Another possibility is that there is a dichotomy between electronic structures corresponding to different parts of the Fermi surface.

Despite the fact that the maximum of the SC dome of CeAu₂Si₂ occurs close to the vanishing of magnetism at $p_c = 22$ GPa, we do not think that the high- p -SC state is mainly spin-mediated. Indeed, the following points portray a different scenario. The unit-cell volume at which T_c^{\max} occurs, the T_c^{\max} value itself, the merging of $T_{\rho,1}^{\max}$ and $T_{\rho,2}^{\max}$ at a relatively high temperature, the proximity of the COV, and its associated NFL

resistivity behavior all illustrate the leading role of valence fluctuations and their criticality at low T , as in the case of $\text{CeCu}_2(\text{Si/Ge})_2$ [16, 18, 29, 31, 61]. Moreover, the collapse of T_N seems to be first-order and we think that the valence crossover COV drives the suppression of magnetism. This does not exclude the usual effect of the competition between Kondo and RudermanKittelKasuyaYosida interactions and the corresponding development of magnetic spin fluctuations at low T . A similar scenario with a first-order collapse of magnetism has been observed for CeCu_2Ge_2 [31]. In spite of the unavoidable p -gradient causing T_N to spread around p_c , we found a steeper drop in CeAu_2Si_2 than in $\text{CeCu}_2(\text{Si/Ge})_2$ alloys, and here again lattice disorder can mitigate the collapse of T_N at p_c . Note that an analogous statement holds for the pressurized lattice CeCu_5Au [62] and its $\text{Ce}(\text{Cu,Au})_6$ alloys [63].

Critical valence fluctuations as SC-paring glue is not in conflict with the absence of traces of any valence transition in microscopic probes on CeCu_2Si_2 [64, 65] and CeCu_2Ge_2 [65, 66] (also because of the low resolution of these techniques). SC is indeed predicted when the critical-end-point temperature is negative ($T_{\text{cr}} < 0$) [29, 61], which means that only a crossover regime occurs at $T \geq 0$. A pressure gradient and sample disorder are expected to lead to an underestimation of T_{cr} deduced from the resistivity scaling, and one can imagine that, in a real crystal, T_{cr} spans over a certain range. Thus, T_{cr} may be positive in some islands, which signifies a trend to a local first-order valence transition with a complex nucleation process. We are now accumulating data to establish a possible relationship between T_{cr} and T_c for HF superconductors.

We remind readers, that two theoretical studies have independently claimed that an orbital transition and its correlated fluctuations mediate the SC in the CeCu_2Si_2 family [67, 68]. We have also supported this possibility for explaining the peculiar magnetic behavior of CeAu_2Si_2 [1], but a recent nonresonant inelastic x-ray scattering study missed a clear signature of an orbital transition in CeCu_2Ge_2 [69]. Nevertheless, considering orbital physics is not unreasonable. For example, the compound $\text{PrTi}_2\text{Al}_{20}$, which shares some of the crucial characteristics shown in Fig. 10, such as the merging of two resistivity contributions at the maximum T_c [70], exhibits nonmagnetic quadrupolar fluctuations [71]. Other

exotic-order fluctuations as the possible pairing mechanism are the magnetic high-rank octopole fluctuation proposed for CeCu_2Si_2 [60] and the various proposals made for the mysterious case of URu_2Si_2 .

V. CONCLUSION

We have performed electric resistivity, thermoelectric power, and ac calorimetry measurements on a CeAu_2Si_2 single crystal under very high pressures and magnetic fields. The resulting p - T phase diagram and the normal-ground-state properties ($H > H_{c2}$) exhibit new key features. A novel magnetic-transition line $T_{\text{M}}^{\text{mod}}$ is associated with modifications of the AF order well below T_N . Temperature- and pressure-driven magnetic instabilities revealed by the pressure and magnetic field dependences of $T_{\text{M}}^{\text{mod}}$ and T_N occur in the vicinity of the SC emergence. Strong correlations between T_N , $T_{\text{M}}^{\text{mod}}$, and T_c are found. The emergence of SC inside the AF phase and the maximum T_c occur in two pressure regimes, around 14 and 22 GPa, respectively, where magnetic instabilities coincide with the quantum critical behavior of the normal-ground-state properties. In CeAu_2Si_2 , p_c and p_{cr} are very close and it is possible that both the suppression of magnetism and the enhanced SC are driven by a valence crossover. The COV line and the NFL behavior around p_{cr} indicate that the p -region of high T_c is governed by the proximity of a critical end point, presumably from a valence transition at negative temperature, and that the SC is probably mediated by critical valence fluctuations. While it appears to be difficult to disentangle the phase diagram of CeAu_2Si_2 , this work has made a salient progress in this direction. Nevertheless, new theoretical work, especially CEF calculations, is required to improve the understanding of the complex magnetic and superconducting properties of CeAu_2Si_2 .

VI. ACKNOWLEDGMENTS

We acknowledge enlightening discussions with J.-P. Brison, D. Braithwaite, G. Knebel, and J. Flouquet and technical support from M. Lopez and S. Müller. This work was financially supported by the Swiss National Science Foundation through Grant No. 200020-137519.

-
- [1] Z. Ren, L. V. Pourovskii, G. Girit, G. Lapertot, A. Georges, and D. Jaccard, *Phys. Rev. X* **4**, 031055 (2014).
 - [2] Z. Ren, G. Girit, G. W. Scheerer, G. Lapertot, and D. Jaccard, *Phys. Rev. B* **91** 094515 (2015).
 - [3] D. Rossi, R. Marazza, and R. Ferro, *J. Less-Common Met.* **66**, P17 (1979).
 - [4] B. H. Grier, J. M. Lawrence, V. Murgai, and R. D. Parks, *Phys. Rev. B* **29**, 2664 (1984).

- [5] V. Murgai, S. Raaen, L. C. Gupta, and R. D. Parks, *Valence Instabilities* P. 537 (North-Holland, Amsterdam, 1982).
- [6] Y. Ota, K. Sugiyama, Y. Miyauchi, Y. Takeda, Y. Nakano, Y. Doi, K. Katayama, N. D. Dung, T. D. Matsuda, Y. Haga, K. Kindo, T. Takeuchi, M. Hagiwara, R. Settai, and Y. Ōnuki, *J. Phys. Soc. Jpn.* **78**, 034714 (2009).

- [7] A. Amato and J. Sierro, *J. Magn. Magn. Mater.* **47-48**, 526 (1985).
- [8] C. S. Garde and J. Ray, *J. Phys.: Condens. Matter* **6**, 8585 (1994).
- [9] P. Link and D. Jaccard, *Physica B* **230-232**, 31 (1997).
- [10] A. Severing, E. Holland-Moritz, and B. Frick, *Phys. Rev. B* **39**, 4164 (1989).
- [11] Z. Ren, G. W. Scheerer, G. Lapertot, and D. Jaccard, *Phys. Rev. B* **94**, 024522 (2016).
- [12] B. H. Grier, J. M. Lawrence, S. Horn, and J. D. Thompson, *J. Phys. C: Solid State Phys.* **21**, 1099 (1988).
- [13] A. Severing, E. Holland-Moritz, B. D. Rainford, S. R. Culverhouse, and B. Frick, *Phys. Rev. B* **39**, 2557 (1989).
- [14] T. Fujiwara, M. Sugi, N. Kimura, I. Satoh, T. Komatsubara, and H. Aoki, *Physica B* **378-380**, 812 (2006).
- [15] A. S. Sefat, A. M. Palasyuk, S. L. Bud'ko, J. D. Corbett, and P. C. Canfield, *J. Solid State Chem.* **181**, 282 (2008).
- [16] A. T. Holmes, D. Jaccard, and K. Miyake, *J. Phys. Soc. Jpn.* **76**, 051002 (2007).
- [17] P. Link, D. Jaccard, and P. Lejay, *Physica B* **225**, 207 (1996).
- [18] A. T. Holmes, D. Jaccard, and K. Miyake, *Phys. Rev. B* **69**, 024508 (2004).
- [19] W. Knafo, R. Settai, D. Braithwaite, S. Kurahashi, D. Aoki, and J. Flouquet, *Phys. Rev. B* **95**, 014411 (2017).
- [20] S. Kawarazaki, M. Sato, Y. Miyako, N. Chigusa, K. Watanabe, N. Metoki, Y. Koike, and M. Nishi, *Phys. Rev. B* **61**, 4167 (2000).
- [21] T. Ebihara, N. Harrison, M. Jaime, S. Uji, and J. C. Lashley, *Phys. Rev. Lett.* **93**, 246401 (2004).
- [22] S. S. Abel'skii and Y. P. Irkhin, *Sov. Phys.-Solid State* **13**, 2035 (1972).
- [23] O. Stockert, E. Faulhaber, G. Zwirnagl, N. Stüßer, H. S. Jeevan, M. Deppe, R. Borth, R. Küchler, M. Loewenhaupt, C. Geibel, and F. Steglich, *Phys. Rev. Lett.* **92**, 136401 (2004).
- [24] G. Knopp, A. Loidl, K. Knorr, L. Pawlak, M. Duczmal, R. Caspary, U. Gottwick, H. Spille, F. Steglich, and A. P. Murani, *Z. Phys. B: Condens. Matter* **77**, 95 (1989).
- [25] G. Knebel, C. Eggert, D. Engelmann, R. Viana, A. Krimmel, M. Dressel, and A. Loidl, *Phys. Rev. B* **53**, 11586 (1996).
- [26] P. Morin, C. Vettier, J. Flouquet, M. Konczykowski, Y. Lassailly, J. M. Mignot, and U. Welp, *J. Low Temp. Phys.* **70**, 377 (1988).
- [27] W. Knafo, D. Aoki, D. Vignolles, B. Vignolle, Y. Klein, C. Jaudet, A. Villaume, C. Proust, and J. Flouquet, *Phys. Rev. B* **81**, 094403 (2010).
- [28] O. Trovarelli, M. Weiden, R. Muller-Reisener, M. Gómez-Berisso, P. Gegenwart, M. Deppe, C. Geibel, J. G. Sereni, and F. Steglich, *Phys. Rev. B* **56**, 678 (1997).
- [29] G. Seyfarth, A. S. Rüetschi, K. Sengupta, A. Georges, D. Jaccard, S. Watanabe, and K. Miyake, *Phys. Rev. B* **85**, 205105 (2012).
- [30] G. Giriat, Z. Ren, P. Pedrazzini, and D. Jaccard, *Solid State Commun.* **209-210**, 55 (2015).
- [31] D. Jaccard, H. Wilhelm, K. Alami-Yadri, and E. Vargoz, *Physica B* **259-261**, 1 (1999).
- [32] T. Park, H. Lee, I. Martin, X. Lu, V. A. Sidorov, K. Gofryk, F. Ronning, E. D. Bauer, and J. D. Thompson, *Phys. Rev. Lett.* **108**, 077003 (2012).
- [33] Around $p_v/2$, polished (cleaved) CeCu_2Si_2 crystals show broad (narrow) resistive T_c with identical bulk T_c established from simultaneous heat capacity and magnetic measurements. G. Scheerer *et al.*, unpublished.
- [34] N. H. Andersen: in *Crystalline Electric Field and Structural Effects in f-Electron Systems*, ed. J. E. Crow, R. P. Guertin, and T. W. Mihalisin (Plenum Press, New York, 1980).
- [35] K. Miyake and O. Narikiyo, *J. Phys. Soc. Jpn.* **71**, 867 (2002).
- [36] G. Neumann, J. Langen, H. Zahel, D. Plümacher, Z. Kle-towski, W. Schlabit, and D. Wohlleben, *Z. Phys. B* **59**, 133 (1985).
- [37] A. Onodera, S. Tsuduki, Y. Ohishi, T. Watanuki, K. Ishida, Y. Kitaoka, and Y. Ōnuki, *Solid State Commun.* **123**, 113 (2002).
- [38] M. Ohmura, K. Sakai, T. Nakano, H. Miyagawa, G. Oomi, I. Sato, T. Komatsubara, H. Aoki, Y. Matsumoto, and Y. Uwatoko, *J. Magn. Soc. Jpn.* **33**, 31 (2009).
- [39] F. Honda, T. Maeta, Y. Hirose, Y. Ōnuki, A. Miyake, and R. Settai, *J. Korean Phys. Soc.* **63**, 345 (2013).
- [40] D. Jaccard, K. Behnia, and J. Sierro, *Phys. Lett. A* **163**, 475 (1992).
- [41] E. Vargoz, Dr. thesis, DPMC, Université de Genève, Geneva (1998).
- [42] D. Jaccard, J. M. Mignot, B. Bellarbi, A. Benoit, H. F. Braun, and J. Sierro, *J. Magn. Magn. Mater.* **47-48**, 23 (1985).
- [43] G. Sparn, W. Lieke, U. Gottwick, F. Steglich, and N. Grewe, *J. Magn. Magn. Mater.* **47-48**, 521 (1985).
- [44] K. Behnia, D. Jaccard, and F. Jacques, *J. Phys.: Condens. Matter* **16**, 5187 (2004).
- [45] V. Zlatić and R. Monnier, *Modern Theory of Thermoelectricity* (Oxford University Press, Oxford, 2014).
- [46] H. Q. Yuan, F. M. Grosche, M. Deppe, C. Geibel, G. Sparn, and F. Steglich, *Science* **302**, 2104 (2003).
- [47] B. Bellarbi, A. Benoit, D. Jaccard, J. M. Mignot, and H. F. Braun, *Phys. Rev. B* **30**, 1182 (1984).
- [48] K. Miyake, O. Narikiyo, and Y. Onishi, *Physica B* **259-261**, 676 (1999).
- [49] Y. Onishi and K. Miyake, *J. Phys. Soc. Jpn.* **69**, 3955 (2000).
- [50] K. Miyake and H. Maebashi, *J. Phys. Soc. Jpn.* **71**, 1007 (2002).
- [51] S. Watanabe, M. Imada, and K. Miyake, *J. Phys. Soc. Jpn.* **75** 043710 (2006).
- [52] M. Ishikawa, N. Takeda, M. Koeda, M. Hedo, and Y. Uwatoko, *Phys. Rev. B* **68**, 024522 (2003).
- [53] A. T. Holmes, D. Jaccard, H. S. Jeevan, C. Geibel, and M. Ishikawa, *J. Phys.: Condens. Matter* **17**, 5423 (2005).
- [54] P. Monthoux, D. Pines, and G. G. Lonzarich, *Nature* **450**, 1177 (2007).
- [55] E. Lengyel, M. Nicklas, H. S. Jeevan, G. Sparn, C. Geibel, F. Steglich, Y. Yoshioka, and K. Miyake, *Phys. Rev. B* **80**, 140513(R) (2009).
- [56] N. D. Mathur, F. M. Grosche, S. R. Julian, I. R. Walker, D. M. Freye, R. K. W. Haselwimmer, and G. G. Lonzarich, *Nature* **394**, 39 (1998).
- [57] O. Stockert, J. Arndt, E. Faulhaber, C. Geibel, H. S. Jeevan, S. Kirchner, M. Loewenhaupt, K. Schmalzl, W. Schmidt, Q. Si, and F. Steglich, *Nat. Phys.* **7**, 119 (2011).
- [58] J. Arndt, O. Stockert, K. Schmalzl, E. Faulhaber, H. S. Jeevan, C. Geibel, W. Schmidt, M. Loewenhaupt, and F. Steglich, *Phys. Rev. Lett.* **106**, 246401 (2011).

- [59] S. Kittaka, Y. Aoki, Y. Shimura, T. Sakakibara, S. Seiro, C. Geibel, F. Steglich, H. Ikeda, and K. Machida, *Phys. Rev. Lett.* **112**, 067002 (2014).
- [60] H. Ikeda, M.-T. Suzuki, and R. Arita, *Phys. Rev. Lett.* **114**, 147003 (2015).
- [61] K. Miyake, *J. Phys.: Condens. Matter* **19**, 125201 (2007).
- [62] H. Wilhelm, S. Raymond, D. Jaccard, O. Stockert, and H. v. Löhneysen, *Science and technology of high pressure*, Proc. of AIRAPT-17, ed. M. H. Manghnani. (Universities Press India, Hyderabad, 2000), p. 697.
- [63] H. v. Löhneysen, *J. Magn. Magn. Mater.* **200**, 532 (1999).
- [64] J.-P. Rueff, S. Raymond, M. Taguchi, M. Sikora, J.-P. Itié, F. Baudelet, D. Braithwaite, G. Knebel, and D. Jaccard, *Phys. Rev. Lett.* **106**, 186405 (2011).
- [65] T. C. Kobayashi, K. Fujiwara, K. Takeda, H. Harima, Y. Ikeda, T. Adachi, Y. Ohishi, C. Geibel, and F. Steglich, *J. Phys. Soc. Jpn.* **82**, 114701 (2013).
- [66] H. Yamaoka, Y. Ikeda, I. Jarrige, N. Tsujii, Y. Zekko, Y. Yamamoto, J. Mizuki, J.-F. Lin, N. Hiraoka, H. Ishii, K.-D. Tsuei, T. C. Kobayashi, F. Honda, and Y. Ōnuki, *Phys. Rev. Lett.* **113**, 086403 (2014).
- [67] K. Hattori, *J. Phys. Soc. Jpn.* **79**, 114717 (2010).
- [68] L. V. Pourovskii, P. Hansmann, M. Ferrero, and A. Georges, *Phys. Rev. Lett.* **112**, 106407 (2014).
- [69] J.-P. Rueff, J. M. Ablett, F. Strigari, M. Deppe, M. W. Haverkort, L. H. Tjeng, and A. Severing, *Phys. Rev. B* **91**, 201108(R) (2015).
- [70] D. Braithwaite, private communication.
- [71] K. Matsubayashi, T. Tanaka, A. Sakai, S. Nakatsuji, Y. Kubo, and Y. Uwatoko, *Phys. Rev. Lett.* **109**, 187004 (2012).

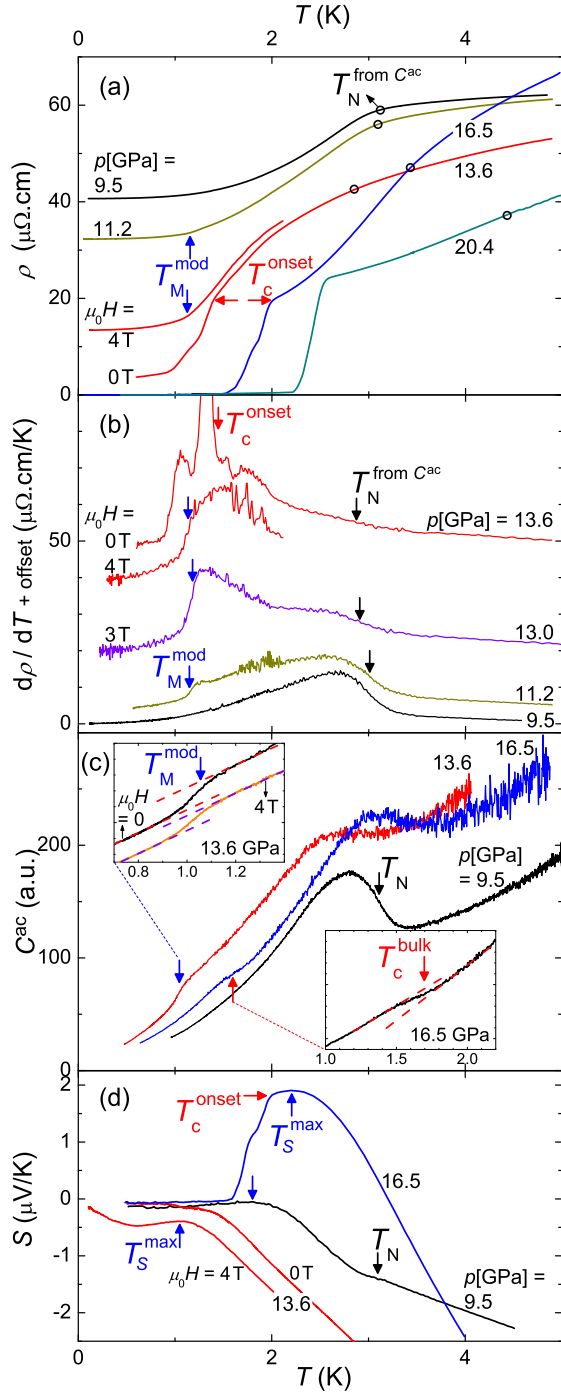


FIG. 2. Multiprobe data of CeAu_2Si_2 at selected pressures and at zero field (otherwise indicated). Anomalies indicated by arrows are described in the text. (a) In-plane resistivity ρ of CeAu_2Si_2 as a function of temperature T . For clarity, offsets of 30 and 20 $\mu\Omega\cdot\text{cm}$ are added to the curves for 9.5 and 11.2 GPa, respectively. The Néel temperature T_N deduced from calorimetry is indicated by circles. (b) $d\rho/dT$ versus T . For clarity, offsets are added to the curves for $p \geq 11.2$ GPa. (c) Ac calorimetry C^{ac} versus T . The upper (lower) inset shows a close up of the curve at 13.6 (16.5) GPa around the temperature $T_{\text{M}}^{\text{mod}}$ ($T_{\text{c}}^{\text{bulk}}$). (d) Thermoelectric power S versus T .

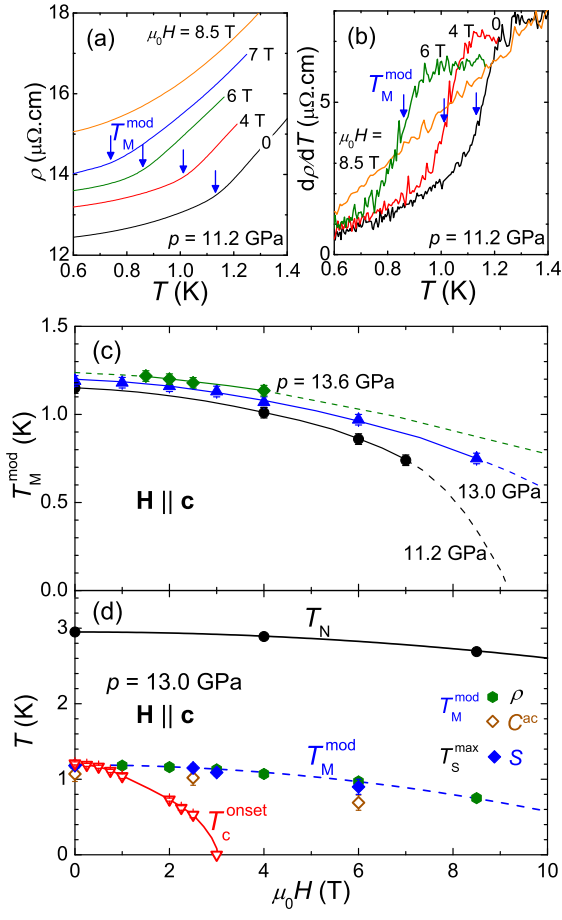


FIG. 3. (a) $\rho(T)$ and (b) $d\rho/dT(T)$ at $p = 11.2$ GPa at different magnetic fields $\mu_0 \mathbf{H} \parallel \mathbf{c}$ up to 8.5 T. T_M^{mod} is indicated by arrows. (c) T_M^{mod} deduced from $d\rho/dT$ versus H applied along \mathbf{c} at $p = 11.2$, 13.0, and 13.6 GPa. Errors are a slightly larger than the symbol size. Lines are guides to the eyes. (d) At $p = 13.0$ GPa, field dependences of the Néel temperature T_N extracted from C^{ac} , T_M^{mod} from C^{ac} and ρ , T_S^{max} from the thermopower, and T_c^{onset} . Lines are guides to the eyes.

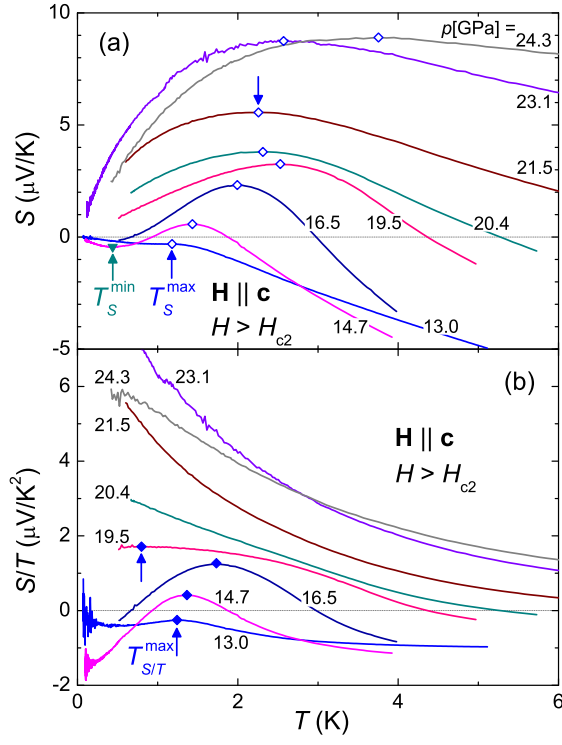


FIG. 4. (a) Normal-state, in-plane thermopower S and (b) S/T of CeAu₂Si₂ as a function of temperature T at different pressures p between 13.0 and 24.3 GPa, measured in magnetic fields higher than the superconducting upper critical field H_{c2} , applied along the c -axis. Arrows/symbols indicate the local extrema at T_S^{\max} , T_S^{\min} , and $T_{S/T}^{\max}$.

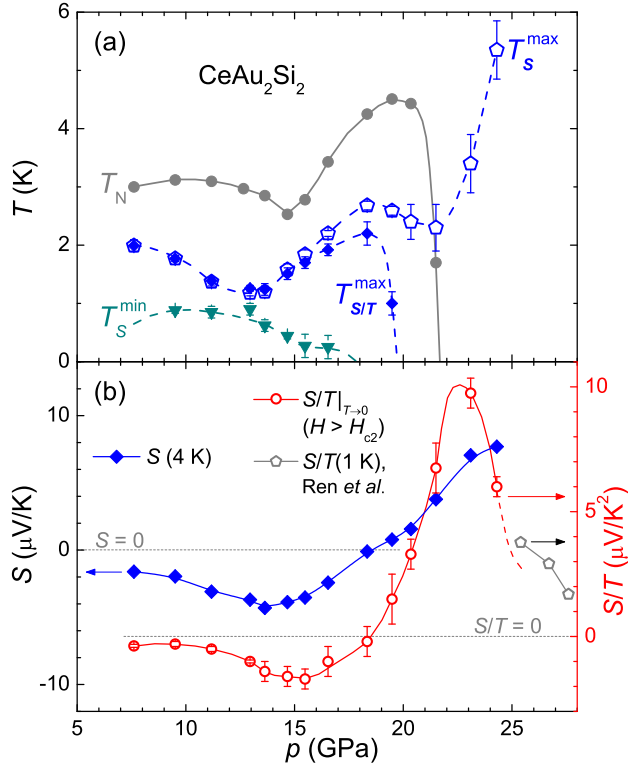


FIG. 5. (a) Pressure dependence of the characteristic temperatures T_N , T_S^{\min} (minimum S), T_S^{\max} (maximum S), and $T_{S/T}^{\max}$ (maximum S/T). (b) Left y-axis: thermopower S at $T = 4$ K. Right y-axis: S/T extrapolated to zero temperature and $S/T(1$ K) from data in Ref. [11]. Lines are guides to the eyes.

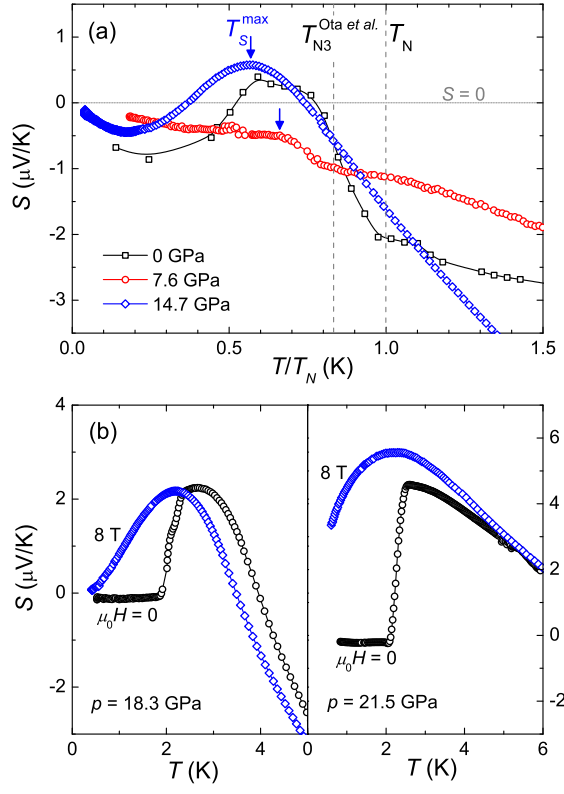


FIG. 6. (a) S versus T/T_N for $p = 0, 7.6$, and 14.7 GPa (same sample as in Ref. [11] for $p = 0$). The vertical dashed lines indicate T_{N3} (at $p = 0$) [6] and T_N . (b) S versus T at $\mu_0 H = 0$ and 8 T for $p = 18.3$ GPa (left panel) and $p = 21.5$ GPa (right panel).

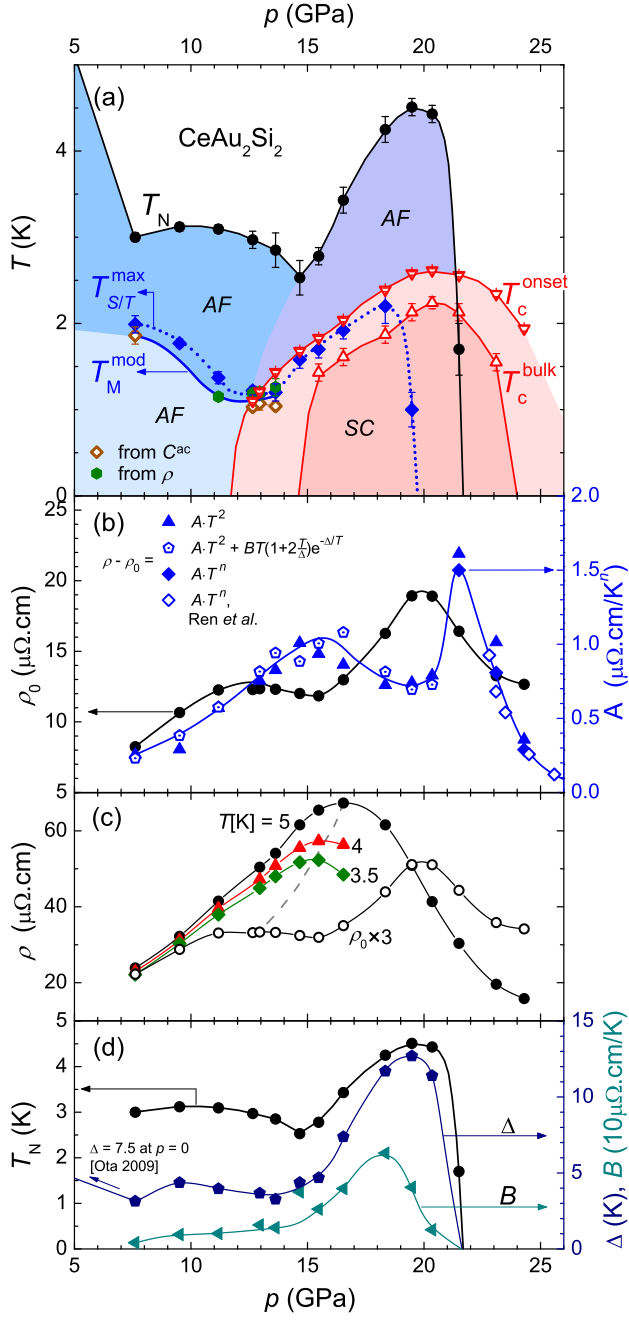


FIG. 7. (a) p - T phase diagram of CeAu₂Si₂ constructed from the multiprobe data for $7 < p < 24.5$ GPa. The Néel temperature T_N is extracted from C^{ac} , T_M^{mod} from C^{ac} and ρ , $T_{S/T}^{\text{max}}$ from the thermopower, T_c^{onset} from ρ , and T_c^{bulk} from C^{ac} . (b) Pressure dependence of the residual resistivity ρ_0 and the power-law coefficient A , extracted from the normal-state resistivity ($H > H_{c2}$) by fitting with $\rho(T) = \rho_0 + A \cdot T^n + B \cdot T(1 + 2T/\Delta)\exp(-\Delta/T)$ ($B = 0$ for $p > p_c$). Data from Ref. [1] are added for comparison. (c) Isothermal ρ vs p at 3.5, 4, and 5 K and $3 \cdot \rho_0$. (d) Pressure dependence of the parameters B and Δ compared with that of T_N .

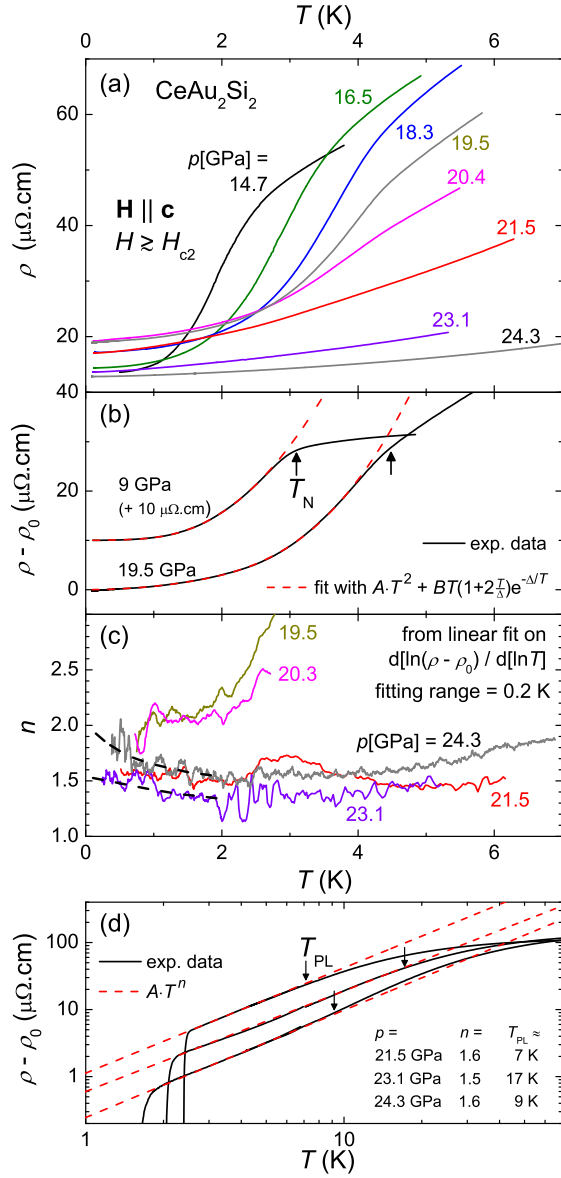


FIG. 8. (a) Normal-state resistivity ρ of CeAu_2Si_2 versus T for $H > H_{c2}$ at selected pressures p . (b) Normal-state $\rho - \rho_0$ vs T at 9 and 19.5 GPa. For clarity, an offset of 10 $\mu\Omega\cdot\text{cm}$ is added to ρ at 9 GPa. Dashed lines represent the fitting described in the text. (c) Temperature dependence of the power-law exponent n extracted by linear fits of $\ln(\rho - \rho_0)$ versus $\ln(T)$ over temperature ranges of 0.2 K. The dashed lines indicate extrapolations of n for $T \rightarrow 0$. (d) log-log plot of normal-state $\rho - \rho_0$ vs T at 21.5, 23.1, and 24.3 GPa. Dashed lines represent $A \cdot T^n$ curves.

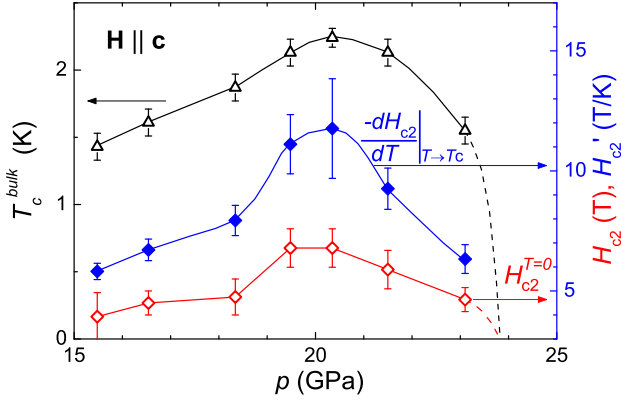


FIG. 9. Pressure dependence of T_c^{bulk} , $H_{c2}(T = 0)$, and $dH_{c2}/dT|_{T=T_c}$. H_{c2} is defined by a 95% drop in resistivity.

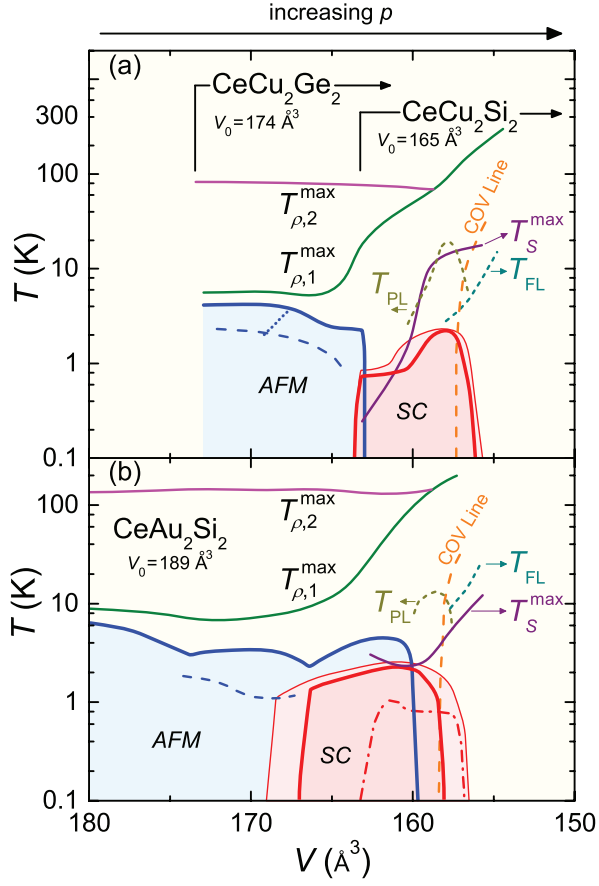


FIG. 10. Schematic unit-cell-volume diagrams of (a) CeCu_2Ge_2 [17, 31, 40, 41] ($V < 173 \text{ \AA}^3$) and CeCu_2Si_2 [18, 29, 42, 43] ($V < 163 \text{ \AA}^3$) and (b) CeAu_2Si_2 (from Refs. [1, 2], and [11], and this work). $V = 189 \text{ \AA}^3$ for CeAu_2Si_2 at $p = 0$. The red dashed-dotted line in (b) indicates the superconducting T_c^{onset} of a self-flux-grown CeAu_2Si_2 crystal [2]. The scale T_{PL} is defined by the temperature above which $\rho(T)$ deviates from a simple power law. The construction of the crossover (COV) line is explained in Ref. [2]. See text for more details.